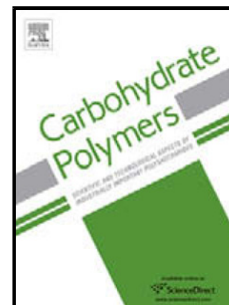


Accepted Manuscript

Title: Dual-responsive Nanoparticles Based on Chitosan for Enhanced Breast Cancer Therapy

Authors: Xuejing Zhang, Shiwei Niu, Gareth R. Williams, Jianrong Wu, Xia Chen, Hong Zheng, Li-Min Zhu



PII: S0144-8617(19)30596-X
DOI: <https://doi.org/10.1016/j.carbpol.2019.05.081>
Reference: CARP 14951

To appear in:

Received date: 16 December 2018
Revised date: 17 May 2019
Accepted date: 28 May 2019

Please cite this article as: Zhang X, Niu S, Williams GR, Wu J, Chen X, Zheng H, Zhu L-Min, Dual-responsive Nanoparticles Based on Chitosan for Enhanced Breast Cancer Therapy, *Carbohydrate Polymers* (2019), <https://doi.org/10.1016/j.carbpol.2019.05.081>

This is a PDF file of an unedited manuscript that has been accepted for publication. As a service to our customers we are providing this early version of the manuscript. The manuscript will undergo copyediting, typesetting, and review of the resulting proof before it is published in its final form. Please note that during the production process errors may be discovered which could affect the content, and all legal disclaimers that apply to the journal pertain.

Dual-responsive Nanoparticles Based on Chitosan for Enhanced Breast Cancer Therapy

Xuejing Zhang^{a,†}, Shiwei Niu^{a,†}, Gareth R. Williams^b, Jianrong Wu^a, Xia Chen^a, Hong Zheng^{c,*} and Li-Min Zhu^{a,*}

^aCollege of Chemistry, Chemical Engineering and Biotechnology, Donghua University, Shanghai, PR China

^bUCL School of Pharmacy, University College London, 29-39 Brunswick Square, London, WC1N 1AX, UK

^cDepartment of Experimental Animal Science, Kunming Medical University, Kunming, PR China

[†]Co-first authors, contributed equally to this work.

* Authors for correspondence: Li-Min Zhu. Tel: +86 13564410208. Email: lzhu@dhu.edu.cn;

Hong Zheng. Tel: +86 13888175273. Email: jiaojianlin66@163.com

Highlights

- Dual-responsive paclitaxel-loaded nanoparticles based on chitosan were fabricated.
- These allowed HA-mediated targeting of CD44-overexpressing breast cancer cells.
- The NPs showed great promise in breast cancer therapy, both in vitro and in vivo.

ABSTRACT

In this study, we report a novel pH and temperature responsive paclitaxel-loaded drug delivery system based on chitosan and di(ethylene glycol) methyl ether methacrylate. This was functionalized with hyaluronic acid to permit active targeting of CD44-overexpressing human breast cancer cells. The resultant HA-CS-g-PDEGMA-PTX nanoparticles (NPs) have small and uniform sizes (~ 170 nm), a high drug loading ($13.6 \pm 1.3\%$) and high encapsulation efficiency ($76.2 \pm 8.5\%$). Cell viability and confocal microscopy experiments demonstrated that the NPs could effectively target and kill MDA-MB-231 human breast cancer cells, but were much less toxic to healthy human umbilical vein endothelial cells. In vivo biodistribution studies in mice showed that the NPs accumulated in the tumor site, while free drug was distributed more widely and rapidly cleared from the body. Histopathological studies revealed that the NPs led to enhanced apoptosis in the tumor site, which resulted in reduced tumor growth. The NPs prepared in this work have great potential for the treatment of breast cancers, and further offer a platform with which to target other cancers.

Keywords: hyaluronic acid; nanoparticles; dual-responsive; anticancer efficacy

1. Introduction

Breast cancer is one of the major causes of death in women, and new treatments are thus much sought after (Torre et al., 2015). Over the past decades, a number of therapeutic interventions have been used for breast tumor treatment, including photodynamic therapy, radiation therapy and chemotherapy (Feng & Chien, 2003), with the latter being the mainstay approach. Unfortunately, chemotherapy has a number of side effects such as hypersensitivity and neurotoxicity (Pearce et al., 2017); these largely arise because it is non-specific and affects healthy tissue as well as cancer cells (Carelle et al., 2002). In addition, many chemotherapeutic drugs have poor water solubility (Barbut, & Chen, 2015; Jin, Pi, & Yang, 2016). Reducing the off-target side effects of chemotherapies would have major benefits for the quality of life of breast cancer patients (de Ligt et al., 2018), and various multifunctional drug delivery systems have been designed to enhance anti-cancer efficacy while reducing the effects of chemotherapeutics on

healthy tissue (Sun et al., 2016; Yang, Tang, & Yin, 2018; Yang et al., 2016). Nanoscale drug delivery systems in particular can lead to the preferential accumulation of drugs within solid tumors, due to the enhanced permeability and retention (EPR) effect (Maeda, 2001; Maeda, Wu, Sawa, Matsumura, & Hori, 2000).

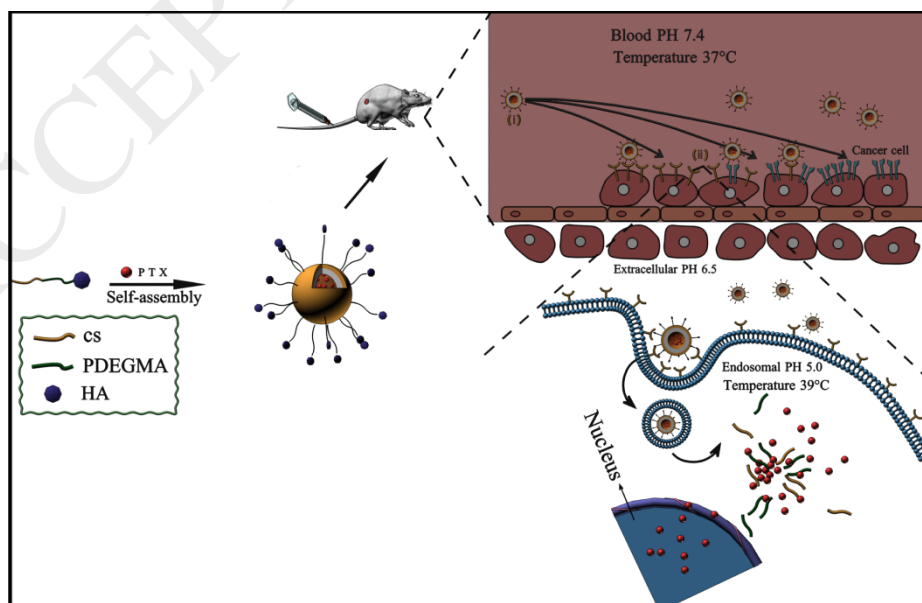
Paclitaxel (PTX) is a broad-spectrum and highly effective anti-cancer drug that acts to stabilize microtubules and inhibit their depolymerization during cell division, leading to apoptosis of tumor cells (Barbuti & Chen, 2015; Okano & Rustgi, 2001). However, its low water solubility and growing drug resistance are major problems (Duan et al., 2017). Responsive drug delivery systems offer one route to overcome these issues. Such systems can allow effective drug targeting and lead to increased circulation times in the blood (Tang, Hua, Cheng, Jiang, & Zhu, 2008). Chitosan (CS) is well established as a suitable material for the fabrication of drug delivery systems, because it is widely available, low-cost, biodegradable, biocompatible, and has low toxicity (Kumar, Muzzarelli, Muzzarelli, Sashiwa, & Domb, 2004; Mao et al., 2001). However, pure CS can only be dissolved in an acidic medium and is not soluble at neutral pH (Hu, Wang, Li, Zeng, & Huang, 2011; Nejati et al., 2018). To improve its properties in this regard, several reports have modified CS with biocompatible materials to obtain a water-soluble polymer. For example, Yang et al. (Yang et al., 2018) grafted ethylene glycol to chitosan, and found the resultant copolymer to have excellent water solubility while retaining the advantages of its parent molecule. Similarly, Chen et al. (Chen, Lin, Wu, & Mi, 2018) used arginine to modify CS and increase its solubility, and found the composite generated to have potential in cancer therapy.

The temperature at the tumor site is slightly higher than that of healthy tissue (by about 1 - 2 °C), and there is the potential to exploit this difference to target therapy (Needham & Dewhirst, 2001). Temperature-responsive polymers which undergo hydrophilic-to-hydrophobic phase transitions at a particular temperature (the so-called lower critical solution temperature (LCST)) have attracted attention for this purpose (Luzon et al., 2010; Xing, Shi, Tian, Sun, & Li, 2018). Poly(di(ethylene glycol) methyl ether methacrylate) (PDEGMA) is one such material (Ramírez-Jiménez, Alvarez-Lorenzo, Concheiro, & Bucio, 2014), and a range of thermosensitive polymers based on PDEGMA have been produced. Li et al. (Li, Pei, Huang, Shi, & Zhang, 2014) synthesized a biodegradable and temperature sensitive dextran/PDEGMA system, while Truong and co-workers (Truong et al., 2016) reported the synthesis of a low-toxicity copolymer of

N-(2-hydroxypropyl) methacrylamide and PDEGMA.

The EPR effect allows a certain degree of tumor targeting, but active targeting can improve specificity further. The latter usually demands the preparation of ligand-functionalized drug delivery systems designed to interact with receptors overexpressed on the surface of cancer cells (Di et al., 2017). CD44 is one such transmembrane protein, and is highly expressed in many cancer cells (Marhaba & Zöllner, 2004). Beyond that, CD44 is a receptor for hyaluronic acid (HA), and the strength of binding between the two is much greater in the case of cancer cells. Thus, HA functionalized drug delivery systems can allow active targeting to cancer cells (Lin, Lu, Wang, Sung, & Mi, 2016; Lv et al., 2018). Exploiting this, Zhong et al. designed HA functionalized pH-responsive PTX prodrug loaded micelles, which they found to be effective in targeting and killing cancerous cells (Zhong et al., 2016).

Here, we develop a platform that combines the pH-sensitive CS and temperature-sensitive PDEGMA to produce a dual responsive system, with the aim of targeting drug release to tumor cells. We further graft the HA to the copolymer in order to provide active targeting properties and decrease the off-target side effects of chemotherapy. A co-polymer of DEGMA and CS (CS-g-PDEGMA) was first prepared by reversible addition fragmentation chain transfer (RAFT) polymerization. CS-g-PDEGMA was next functionalized with HA to yield HA-CS-g-PDEGMA. PTX loaded HA-CS-g-PDEGMA nanoparticles (HA-CS-g-PDEGMA-PTX NPs) were then self-assembled in water. This approach is illustrated in Scheme 1. The products were fully characterised, and explored for their efficacy against cancer both in vitro and in vivo.



Scheme 1. A schematic illustrating the approach used to develop targeted anti-cancer medicines in this work.

2. Materials and methods

2.1 Materials

Chitosan (CS, degree of deacetylation = 95.2%, Mw 200 kDa) was obtained from the SinoPharm Chemical Reagent Co., Ltd (Shanghai, China).

S²-1-dodecyl-S²-(a,a'-dimethyl-a''-acetic acid) trithiocarbonate (DDATC), azobisisobutyronitrile (AIBN) and paclitaxel (PTX) were purchased from the Aladdin Company (Shanghai, China). Di(ethylene glycol) methyl ether methacrylate (DEGMA), fluorescein isothiocyanate (FITC), 4-(dimethyl-amino) pyridine (DMAP), 1-(3-dimethylamino-propyl)-3-ethylcarbodiimide hydrochloride (EDC·HCl), N,N-dicyclohexylcarbodiimide (DCC), N-hydroxysuccinamide (NHS), 3-(4, 5-dimethyl-thiazol-yl)-2, 5-diphenyltetrazolium bromide (MTT), calcein-AM, propidium iodide (PI) and phosphate buffered saline (PBS) were sourced from Sigma-Aldrich (St. Louis, MO, USA). N,N-dimethyl formamide (DMF) was distilled under reduced pressure from calcium hydride and stored over molecular sieves (4 Å). Hyaluronic acid (HA, molecular weight 5 kDa) was purchased from the Shandong Freda Biopharmaceutical Co. Ltd. (Qingdao, China), and DiR (1,10-dioctadecyl-3,3,30,30-tetramethylindotricarbocyanine iodide) from Biotium (Fremont, CA, USA). 4',6-diamidino-2-phenylindole (DAPI) was obtained from the Dingguochangsheng Biotechnology Co. Ltd. (Beijing, China). Dialysis bags (molecular weight cutoff of 3500 Da) were purchased from Yuanye Biotechnology Co. Ltd (Shanghai, China). MilliQ water (resistivity > 18.2 MΩ cm⁻¹) was generated using a MilliQ academic water purification system (Millipore, Burlington, MA, USA). All other chemicals and solvents used were of at least analytical grade.

MDA-MB-231 cells and human umbilical vein endothelial (HUVEC) cells were purchased from the Type Culture Collection of the Chinese Academy of Sciences (Shanghai, China). Dulbecco's Modified Eagle Medium (DMEM), fetal bovine serum (FBS), penicillin, streptomycin and trypsin-EDTA were obtained from Gibco (Carlsbad, CA, USA).

Female nude mice (18-20 g, 5-6 weeks old) and Sprague-Dawley (SD) rats were supplied by the Animal Center of Kunming Medical University (Kunming, China) and housed under specific pathogen-free conditions at 20–22 °C. All animal care and handling was conducted in accordance with the Guide for the Care and Use of Laboratory Animals published by the US National Institutes of Health (NIH Publication No. 8523, revised 1985). The experimental protocols were

reviewed and approved by the Animal Care and Use Committee of Kunming Medical University (ref: KMMU 2015002).

2.2 Synthesis of HA-CS-g-PDEGMA-PTX NPs

CS (5 g) was completely dissolved in 1.0 % w/w acetic acid solution (250 mL). 250 mL of absolute ethanol and 0.5 mL of acetic anhydride were then added, and the mixture was stirred at room temperature for 12 h. 10 % w/w NaOH in water (20 mL) was then poured into the resulting mixture. The precipitate was filtered and lyophilized to give an acetylated product, N-acetyl CS. Subsequently, N-acetyl CS (0.292 g) was dissolved in DMF (40 mL) and reacted with DDATC (0.37 g), DCC (0.205 g) and DMAP (0.015 g) under stirring at room temperature for 40 h. The resultant mixture was poured into ice water and lyophilized to give a yellow powder, CS-RAFT.

To generate the copolymer a solution of CS-RAFT (0.0468 g) was prepared in DMF (10 mL), with stirring for 4 h under nitrogen to ensure all solid material had completely dissolved. AIBN (0.0032 g) and DEGMA (1.5 g) were added, and the mixture obtained was stirred at 60 °C for 24 h under nitrogen, followed by pouring into ice-cold ether (50 mL). Precipitation was allowed to proceed for 12 h, followed by filtration and lyophilization to obtain N-acetyl CS-g-PDEGMA. The acetyl groups were removed by stirring N-acetyl CS-g-PDEGMA in aqueous NaOH (15.0M, 10 mL) for 48 h at room temperature. The mixture was activated with an EDC / NHS (EDC 100 mg, NHS 60 mg) solution in DMF (10 mL) for 2 h and then HA (14.28 mg/mL, 1.5 mL) was added and reaction allowed to proceed with stirring at room temperature for 12 h.

Finally, PTX-loaded NPs (HA-CS-g-PDEGMA-PTX) were prepared by dialysis. HA-CS-g-PDEGMA (100 mg) was dissolved in water (5 mL) and PTX (20 mg) was dissolved in anhydrous ethanol (5 mL). The PTX solution was added to the HA-CS-g-PDEGMA solution, and the mixture stirred at room temperature for 24 h. It was next sealed in a dialysis bag with a 3500 Da MW cutoff, dialyzed against water at 25 °C for 72 h, and centrifuged at 3000 rpm for 1 h to remove any unencapsulated drug. An analogous method, except with CS-g-PDEGMA, was used to generate the HA-free CS-g-PDEGMA-PTX NPs.

2.3. Characterization of NPs

Fourier transform infrared (FT-IR) spectroscopy was performed with a Nicolet Nexus 670 spectrometer (Thermo Fisher, Waltham, MA). Scans were recorded over 3500–500 cm^{-1} with resolution of 2 cm^{-1} and 64 scans collected. ^1H NMR spectra were measured on a Bruker DRX

400 nuclear magnetic resonance spectrometer (Bruker, Rheinstetten, Germany) using DMSO-d₆ as the solvent. Transmission electron microscopy (TEM) was performed on a JEM 1200EX instrument (JOEL, Tokyo, Japan). Dynamic light scattering (DLS) data were obtained on a BI-200SM instrument (Brookhaven Instruments, Holtsville, NY). Samples were prepared at a concentration of 0.5 g/L, and filtered through a 0.45 μm membrane before DLS was performed at 25 °C. The lower critical solution temperature (LCST) of the nanoparticles was recorded using a LAMBDA 35, UV-vis spectrophotometer (PerkinElmer, Waltham, MA).

The percentage encapsulation efficiency (EE) and drug loading (DL) of PTX in HA-CS-g-PDEGMA-PTX NPs were quantified by high performance liquid chromatography (HPLC). The system consisted of a CTA-6A auto-sampler and LC-6A pumps (Shimadzu, Tokyo, Japan). A C₁₈ column (3.9× 150 mm, 10 μm) was employed, with a methanol/water mixture (44/55 v/v) forming the mobile phase. The flow rate was 1 mL/min. PTX was quantified at a wavelength of 227 nm. The percentage EE and DL were calculated as follows:

$$EE = (PTX_n - PTX_m / PTX_n) \times 100\%$$

$$DL = (PTX_n - PTX_m) / \text{Total mass of nanoparticles} \times 100\%$$

where PTX_n is the total mass of PTX used in the preparation of the NPs and PTX_m is the un-encapsulated drug remaining in the supernatant.

2.4. In vitro drug release

The PTX release from the drug-loaded HA-CS-g-PDEGMA NPs was explored at different pH (5.0 or 7.4) and temperatures (37°C or 40°C) using a dialysis method.

HA-CS-g-PDEGMA-PTX NPs (containing 0.5 mg PTX) were placed into a dialysis bag (molecular weight cutoff: 3500 Da) and dialyzed against 25 mL of PBS (pH 5.0 or 7.4) with magnetic stirring (150 rpm) throughout all experiments. At periodic time intervals, aliquots (1 mL) were removed and replaced with preheated fresh medium to maintain a constant volume. The aliquots were centrifuged at 10,000 rpm for 30 minutes, and the amount of PTX in the supernatant quantified by HPLC. Each experiment was performed in triplicate.

2.5. In vitro cytotoxicity

The cytotoxicity of the HA-CS-g-PDEGMA-PTX NPs against MDA-MB-231 tumor cells was analyzed using the MTT assay. HUVEC cells were employed as a healthy cells control. MDA-MB-231 cells or HUVEC cells were cultured in DMEM medium containing 10% v/v FBS,

penicillin (100 U/mL), and streptomycin (100 mg/mL). 1×10^4 cells/well (in 150 μ L of medium) were seeded in each well of a 96-well plate and incubated for 24 h. 20 μ L solutions or suspensions of the various formulations (free PTX, HA-CS-g-PDEGMA and HA-CS-g-PDEGMA-PTX) in PBS were then added to the wells, to give final PTX concentrations ranging from 0.1 to 1000 μ g/mL. In the case of HA-CS-g-PDEGMA, the same mass of polymer as for the HA-CS-g-PDEGMA-PTX experiments was used. The plate was then incubated in a humidified atmosphere for another 24 h. 20 μ L of the MTT reagent (5 mg /mL in PBS) was added to each well and the plate incubated for 4 h at 37 °C in the dark. Finally, DMSO (200 μ L) was added and the absorbance at 490 nm measured using a microplate reader (PowerWave XS, Bio-Tek, Winooski, VT, USA). Three independent experiments were performed with five replicates in each.

To further demonstrate the cytotoxicity of the NPs, the calcein-AM/PI double-labeling method was used. MDA-MB-231 cells were seeded into six-well plates (2 mL, 10^5 cells/well) and incubated in a humidified atmosphere for 24 h. The medium was replaced with a NP suspension (50 mg/mL in PBS) and the plate incubated for a further 24 h. After this, the cells were washed with PBS (1 mL) three times. The cells were subsequently stained with a mixed calcein-AM and PI solution for 15 min. Apoptotic (red) and living cells (green) were imaged under an inverted fluorescent microscope (TE-2000U, Nikon Tokyo, Japan).

2.6. Confocal laser scanning microscopy (CLSM)

To demonstrate the targeting capacity of HA, cellular uptake of the NPs was explored by CLSM. HA-CS-g-PDEGMA-PTX NPs and CS-g-PDEGMA-PTX NPs were labeled with FITC as follows. The NPs were dissolved in methanol, and FITC added to the mixture (NPs: FITC ratio: 5:2 w/w). This was stirred in the dark at room temperature for 24 h, then dialyzed against water at 25 °C for 72 h to obtain labelled NPs. Cells were incubated at 37°C and detached after reaching 70-80% confluence. For CLSM work, MDA-MB-231 cells and HUVEC cells were seeded into 24-well plates at a density of 1×10^4 cells per well (in 2 mL of medium), and incubated for 24 h. Next the cells were washed three times with PBS (pH 7.4, 1 mL), HA-CS-g-PDEGMA-PTX or CS-g-PDEGMA-PTX NPs (200 μ L, 1 mg/mL) and fresh medium (1.5 mL) were added, and the plate incubated for 2 h. Finally, the cells were washed with PBS (pH 7.4, 1 mL) and fixed with 1 mL of a 2.5% v/v glutaraldehyde solution for 10 min. The nuclei were stained with DAPI (50 mg/mL, 100 μ L), and the cells examined by CLSM (FV1000 microscope, Olympus, Tokyo,

Japan).

2.7 In vitro hemolysis assay

Fresh blood samples were obtained from healthy male SD rats and red blood cells (RBCs) were separated by centrifuging at a speed of 1500 rpm for 15 min at 4 °C. The supernatant was discarded and the RBCs were resuspended in saline to a concentration of 2 % w/v.

HA-CS-g-PDEGMA-PTX NPs, CS-g-PDEGMA-PTX NPs or free PTX were serially diluted to different concentrations and incubated with the RBC suspension at 37 °C for 2 h. The absorbance of the supernatant was measured using a microplate reader (Power Wave XS, Bio-Tek, Winooski, VT, USA) at 541 nm. The controls for zero (blank) and 100% hemolysis comprised RBCs suspended in PBS and 1% Triton X-100, respectively. Each measurement was conducted in triplicate.

2.8. In vivo biodistribution

In order to visualize the metabolic fate of HA-CS-g-PDEGMA-PTX NPs in vivo, imaging was undertaken using a Maestro™ in vivo imaging system (CRi Inc, Woburn, MA, USA). A near infrared fluorescence emission dye (DiR) was encapsulated in the nanoparticles in place of PTX (giving HA-CS-g-PDEGMA-DiR). A MDA-MB-231 tumor-bearing mice model was constructed by injecting 100 µL of a cell suspension (containing $\sim 4 \times 10^6$ MDA-MB-231 cells) subcutaneously into the right flank area of nude mice. Sixteen tumor-bearing mice were randomly divided into two groups. HA-CS-g-PDEGMA-DiR NPs or free DiR were intravenously injected when the tumor volume (calculated as $M \times N^2/2$; M: tumor length, N: tumor width) reached approximately 100 mm³. Fluorescence scans were performed at periodic time intervals (1, 4, 8, 12 and 24 h) after injection. After in vivo imaging, the mice were sacrificed by carbon dioxide asphyxiation. The tumor, heart, liver, spleen, lungs and kidneys were harvested and washed with cold saline for further ex vivo fluorescence imaging of DiR (Ke et al., 2018; Tang et al., 2017).

2.9. In vivo antitumor efficacy

100 µL of a MDA-MB-231 cells suspension (containing $\sim 4 \times 10^6$ MDA-MB-231 cells) was injected subcutaneously into the right flank area of nude mice. When the tumor volume reached ca. 100 mm³, mice were randomly divided into 3 groups (8 mice per group) and given intravenous injections of saline, free PTX or HA-CS-g-PDEGMA-PTX NPs (7 mg/kg of PTX equiv.) every two days for 60 days. The body weight of the mice was monitored every two days and the survival

curve evaluated by Kaplan-Meier analysis (Martinez-Garcia et al., 2018).

2.10. Histological analyses of tumor apoptosis

After treatment for 30 days, one mouse in each group was sacrificed by carbon dioxide asphyxiation. The tumor and major organs were excised and fixed in 4% formaldehyde for 48 h. They were then embedded in paraffin and cut into 5 μ m slices. These sections were stained with hematoxylin and eosin (H&E) and studied under a light microscope. In order to observe cell apoptosis in the tumor tissue, sections were stained with a terminal deoxynucleotidyl transferase dUTP nick end labeling (TUNEL) apoptosis detection kit (Beyotime, Beijing, China) according to the manufacturer's instructions, followed by observation by light microscopy.

2.11. Statistical analysis

All experiments were repeated at least three times. Statistical analysis was conducted using the Student's T test for comparison of two groups, and one-way ANOVA followed by Tukey's post hoc test for multiple groups. The SPSS 19.0 software (SPSS, Chicago, IL, USA) was employed for this. P Values less than 0.05 were considered to be statistically significant.

3. Results and discussion

3.1. Preparation and characterization of HA-CS-g-PDEGMA-PTX NPs

Fig. 1A depicts the infrared spectra of CS, DEGMA, HA and HA-CS-g-PDEGMA. The characteristic C₆-OH and C₃-OH bands of CS appear at 1015 cm⁻¹ and 1052 cm⁻¹ in the spectrum of the raw material. DEGMA displays peaks at 2885 cm⁻¹ (CH₃ stretching), 1722 cm⁻¹ (C=O stretching), and 1630 cm⁻¹ (C=C). HA has absorption bands at 1615 cm⁻¹ and 3448 cm⁻¹ which can be ascribed to the -NHCO and -COOH groups. In the spectrum of HA-CS-g-PDEGMA, the DEGMA C=O absorption band at 1725 cm⁻¹ and the HA -NHCO vibration at 1620 cm⁻¹ can still be seen, and at 2880 cm⁻¹ the characteristic absorption bands of saturated -CH₂ groups are visible. The DEGMA C=C stretch also appears to have disappeared. All these observations indicate the successful preparation of HA-CS-g-PDEGMA.

¹H NMR spectroscopy (Fig. 1B) was used to confirm the findings from IR spectroscopy. The spectra of CS, DEGMA and HA are provided in the Supplementary Information (Fig. S1). The spectrum of HA-CS-g-PDEGMA shows characteristic resonances from all its components. The peaks of the CH₂ protons of CS can be seen at 3.00–3.50 ppm, while the PDEGMA aliphatic protons are shown at 1.82–2.00 ppm and 0.50–0.75 ppm. The HA peaks are hard to resolve (given

its small w/w content in the overall polymer), but appear to lie between 3.5 and 4.0 ppm.

The morphologies of the HA-CS-g-PDEGMA-PTX NPs were investigated by TEM (Fig. 1C). The NPs exhibit spherical structures and uniform sizes (170 ± 16 nm). The hydrodynamic diameter recorded by DLS was approximately 190 ± 18 nm. (Fig. 1D), somewhat larger than that observed by TEM as a result of the particles being hydrated when in suspension. The HA-CS-g-PDEGMA-PTX NPs retain the thermosensitive properties of PDEGMA, and display a phase transition at 27-37°C with an LCST of 35°C (Fig. 1E). HPLC analysis indicated that the NPs have a high drug loading ($13.6 \pm 1.3\%$) and encapsulation efficiency ($76.2 \pm 8.5\%$). The size of the NPs should allow them to exploit the EPR effect to become localized in tumor tissue, and the drug loading and encapsulation efficiency are similar to a previous report by Niu et al., who obtained values of 13.5 and 74.3%, respectively (Niu et al., 2018).

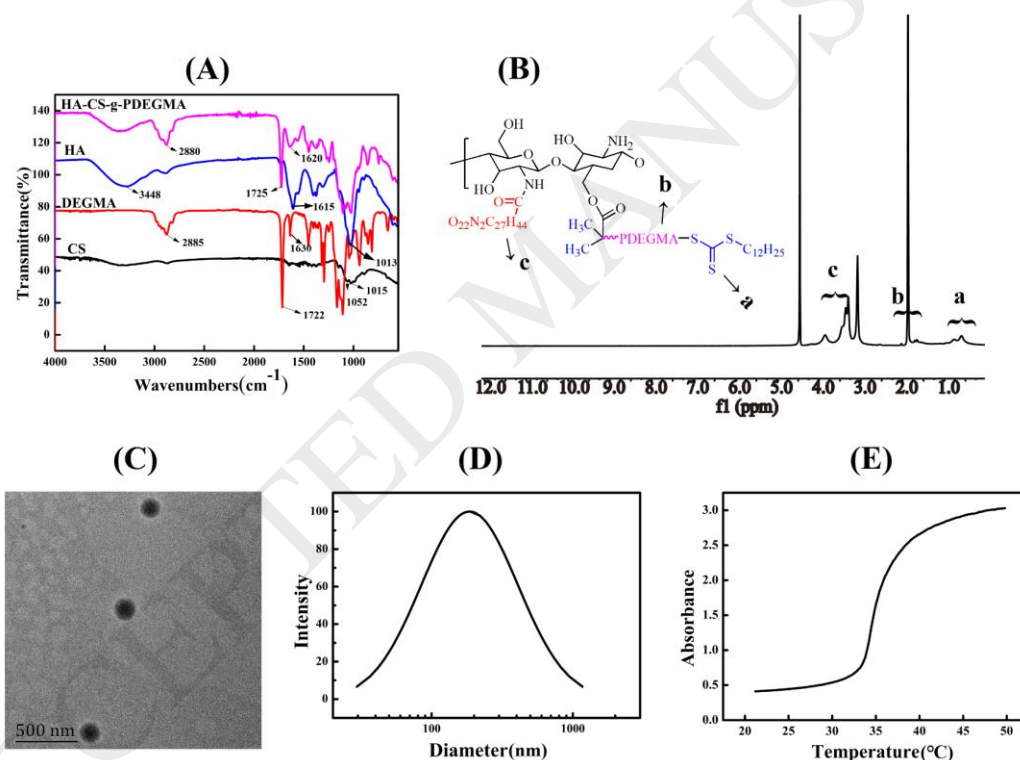


Fig. 1. Synthesis and characterization of HA-CS-g-PDEGMA-PTX NPs. (A) FT-IR spectra. (B) ¹H NMR spectrum in DMSO-d₆. (C) A TEM image. (D) The particle size distribution as measured by DLS. (E) The change in absorbance at 500 nm of an aqueous solution of HA-CS-g-PDEGMA-PTX with temperature.

3.2. In vitro drug release

Drug release from the HA-CS-g-PDEGMA-PTX NPs was explored in vitro at different pH values (pH = 5.0 or 7.4) and temperatures (37 or 40°C). The results are presented in Fig. 2A. It can

be seen that the rate and extent of release of PTX are lower at pH 7.4 than at pH 5.0. Reduced release was observed at pH 7.4 likely to be because PTX was encapsulated in the core of insoluble CS-based nanoparticles. In contrast, PTX has a significantly enhanced release at pH 5.0, as a result of the dissolution of CS in acidic environments.

The drug release rate is faster in the initial stages and gradually decreases as the release time is prolonged. Fig. 2A also shows a significant change in PTX release from HA-CS-g-PDEGMA-PTX NPs at different temperatures. Within 48 h only approximately 47% of PTX was released at 37 °C, but this increases to 73% at 40° C. When the temperature is increased the PTX release rate is enhanced due to the collapse of the structure of the NPs as the PDEGMA component undergoes a hydrophilic-to-hydrophobic transition. Given that a tumor is slightly warmer and more acidic than the usual physiological conditions, these NPs could be potent as anti-cancer drug delivery systems.

3.3 Blood compatibility

To determine the biocompatibility of NPs, a hemolysis assay was performed. As shown in Fig. 2B, the extent of hemolysis is dose-dependent. Free PTX induced RBC lysis even at very low concentrations, whereas 250 µg/ml suspensions of the HA-CS-g-PDEGMA and HA-CS-g-PDEGMA-PTX NPs had much lower hemolytic activity (< 10 %). The HA-CS-g-PDEGMA NPs thus have excellent blood compatibility. The values found here are similar to those noted by Zhang et.al. (Zhang et al., 2016), who synthesized redox-sensitive micelles and observed <5% hemolysis.

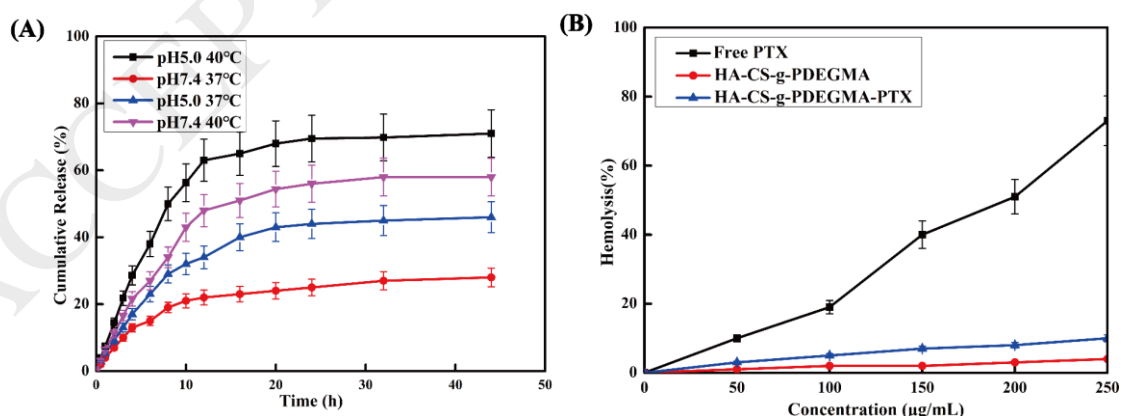


Fig. 2. In vitro PTX release in PBS at different pH and different temperatures, measured with a dialysis method (n=3, mean \pm S.D.). (B) Hemolytic activity of free PTX, HA-CS-g-PDEGMA and HA-CS-g-PDEGMA-PTX NPs on rat red blood cells (n = 3, mean \pm S.D.).

3.4. In vitro cytotoxicity

The cytotoxicity of free PTX, HA-CS-g-PDEGMA and HA-CS-g-PDEGMA-PTX NPs in vitro was assessed with the MTT assay. The HUVEC data in Fig. 3A reveal that the toxicity of the HA-CS-g-PDEGMA NPs in HUVEC cells is negligible at concentrations of 0.1 up to 1000 $\mu\text{g/ml}$ ($> 96\%$ viability). In contrast, the cell viability decreases with an increasing concentration of free PTX or HA-CS-g-PDEGMA-PTX NPs. The viability is higher with the NPs than with free PTX, however, which is promising for the development of targeted therapeutics. Similarly, the blank nanocarrier HA-CS-g-PDEGMA NPs also have negligible cytotoxicity to cancerous MDA-MB-231 cells, and again the HA-CS-g-PDEGMA-PTX NPs lead to higher toxicity than the free drug at PTX concentrations ranging from 0.1 to 1000 $\mu\text{g/mL}$. Further, the HA-CS-g-PDEGMA-PTX NPs are more cytotoxic to MDA-MB-231 cells than HUVEC cells; this can be attributed to active targeting of HA receptors by HA-CS-g-PDEGMA-PTX NPs. These findings concur with a previous study by Li et al. (Li et al., 2013), who reported chitosan/hyaluronic acid-paclitaxel (CS/HA-PTX) NPs prepared by coating CS onto HA-PTX NPs.

Calcein-AM/PI double staining (Fig. 3C) showed little apoptosis in cells treated with HA-CS-PDEGA NPs, while HA-CS-PDEGA-PTX NPs caused significant apoptosis, notably more than free PTX. These data indicate that inhibition of cell proliferation by HA-CS-PDEGA-PTX NPs is at least in part associated with the induction of apoptosis.

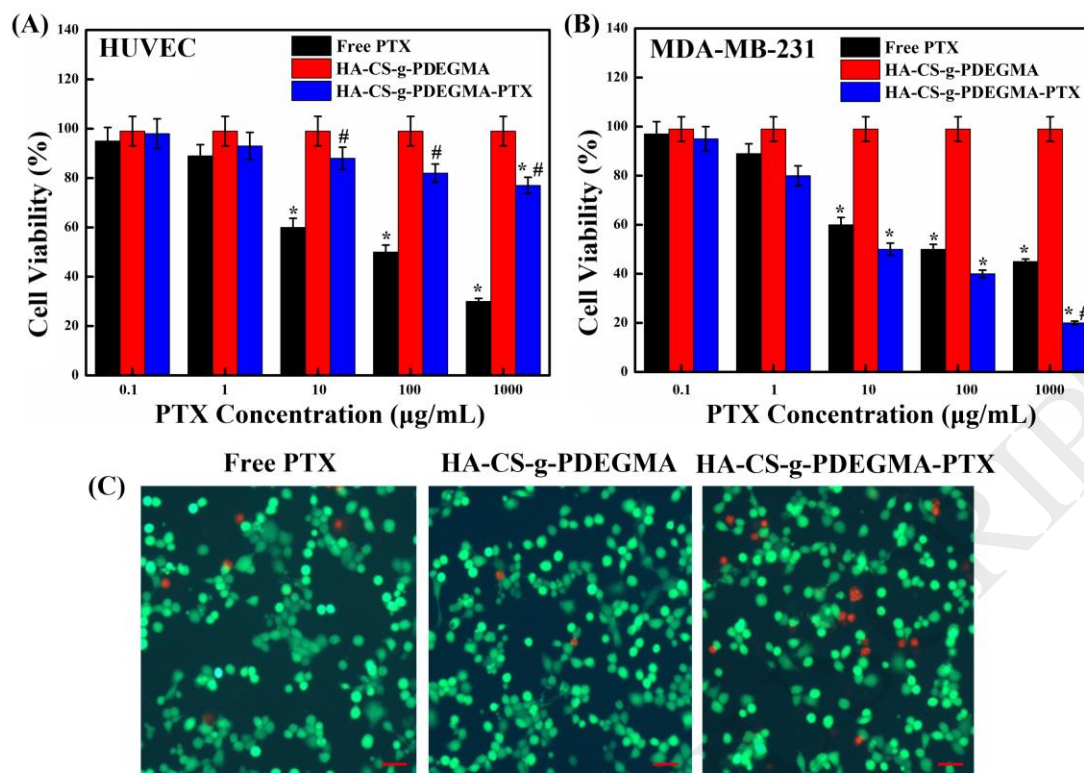


Fig. 3. Cell viability of (A) HUVEC and (B) MDA-MB-231 cells after incubation with free PTX, HA-CS-g-PDEGMA and HA-CS-g-PDEGMA-PTX for 24 h. (C) Fluorescence images of calcein-AM (green)/PI (red) double stained cells (scale bars = 50 μm). Apoptotic cells are stained red. *denotes $p < 0.05$, compared with HA-CS-g-PDEGMA, # denotes $p < 0.05$, compared with Free PTX.

3.5. In vitro cellular uptake

To assess the in vitro cellular uptake of the nanoparticles, they were incubated with MDA-MB-231 cells (significantly overexpressing CD44) and HUVEC cells (no overexpression of CD44). The PTX-loaded nanoparticles were labeled with FITC (green fluorescence), the nuclei were stained with DAPI (blue), and the distribution of NPs was observed by CLSM (Fig. 4). The FITC fluorescence intensity of MDA-MB-231 cells incubated with HA-CS-PDEGA-PTX NPs is notably higher than those exposed to CS-PDEGA-PTX NPs. Only a small amount of fluorescence was seen in HUVEC cells treated with HA-CS-PDEGA-PTX NPs. It can also be seen that the HA-functionalized nanoparticles produced green fluorescence in the cytoplasm of MDA-MB-231 cells, and this fluorescence is closer to the nucleus than in HUVEC cells. These data indicate that HA-functionalized nanoparticles are taken up to a greater extent by MDA-MB-231 cells, as a result of the HA targeting.

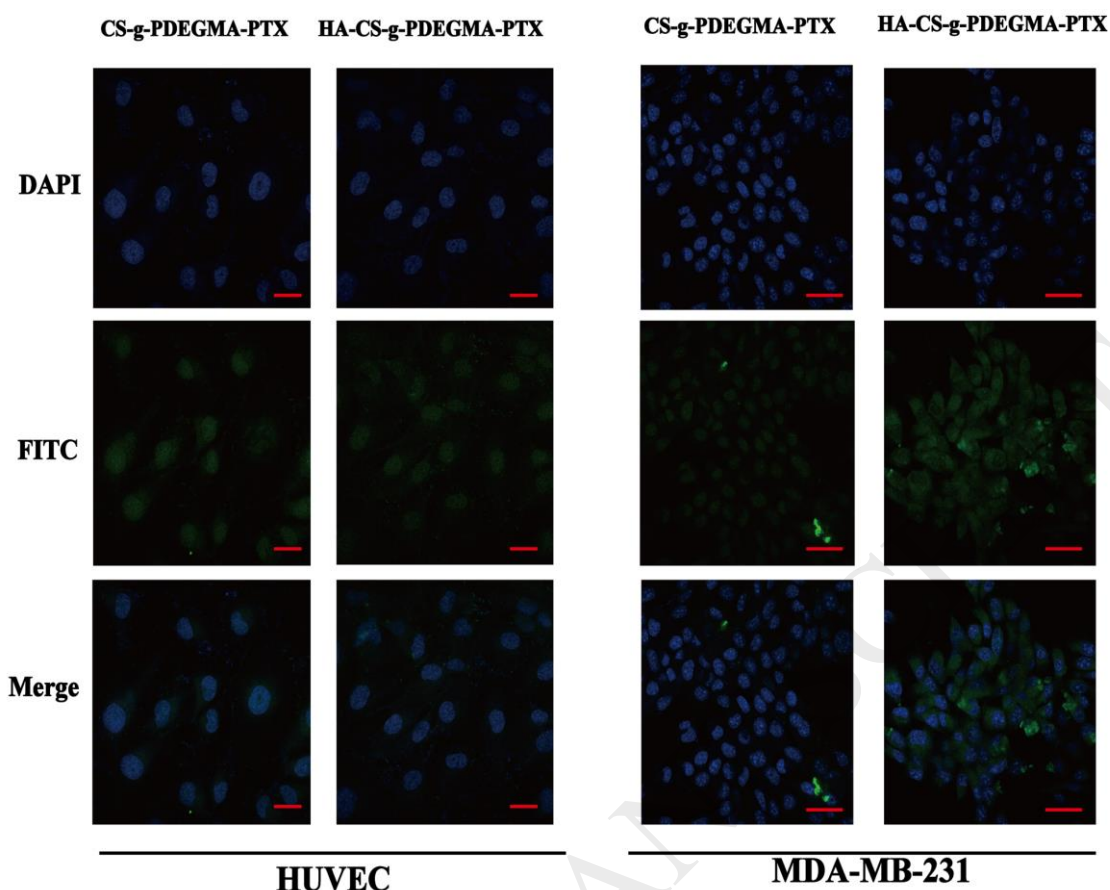


Fig. 4. The results of cellular uptake assays on MDA-MB-231 and HUVEC cells (scale bars = 50 μ m).

3.6. In vivo and ex vivo fluorescence imaging

DiR was used to track the distribution of NPs in tumor-bearing mice, and the real-time biodistribution behavior of free DiR and HA-CS-g-PDEGMA-DiR NPs monitored (Fig. 6A). The images show that the HA-CS-g-PDEGMA-DiR NPs had accumulated at the tumor site 1 h after injection, and the signal intensity continued to increase up to 8 h, after which it was maintained for the remainder of the 24 h monitoring period. In contrast, in the free DiR group, a slight fluorescence could be observed at the tumor site after 1h but this had disappeared at 8 h, probably due to rapid clearance from the blood. There appears to be a tendency for the NPs to accumulate in the tail 24h after injection; the reason for this is not clear, but it may be that the animal used for this image was injected in the back of the tail, and aggregation of NPs in the vein led to this effect. To further confirm the distribution of the NPs, mice were sacrificed 24 h post-injection. The heart, liver, spleen, lungs, kidneys, and tumor were harvested and imaged ex vivo (Fig. 6B). The DiR-loaded NPs are seen to have accumulated in the tumor, while the free DiR was almost all in the liver. The fluorescence intensity at the tumor site was ca. 3-fold higher with the NPs than with

free DiR (Fig. 6C). Fluorescence in all the major organs is also notably lower with the NPs than free DiR ($p < 0.05$).

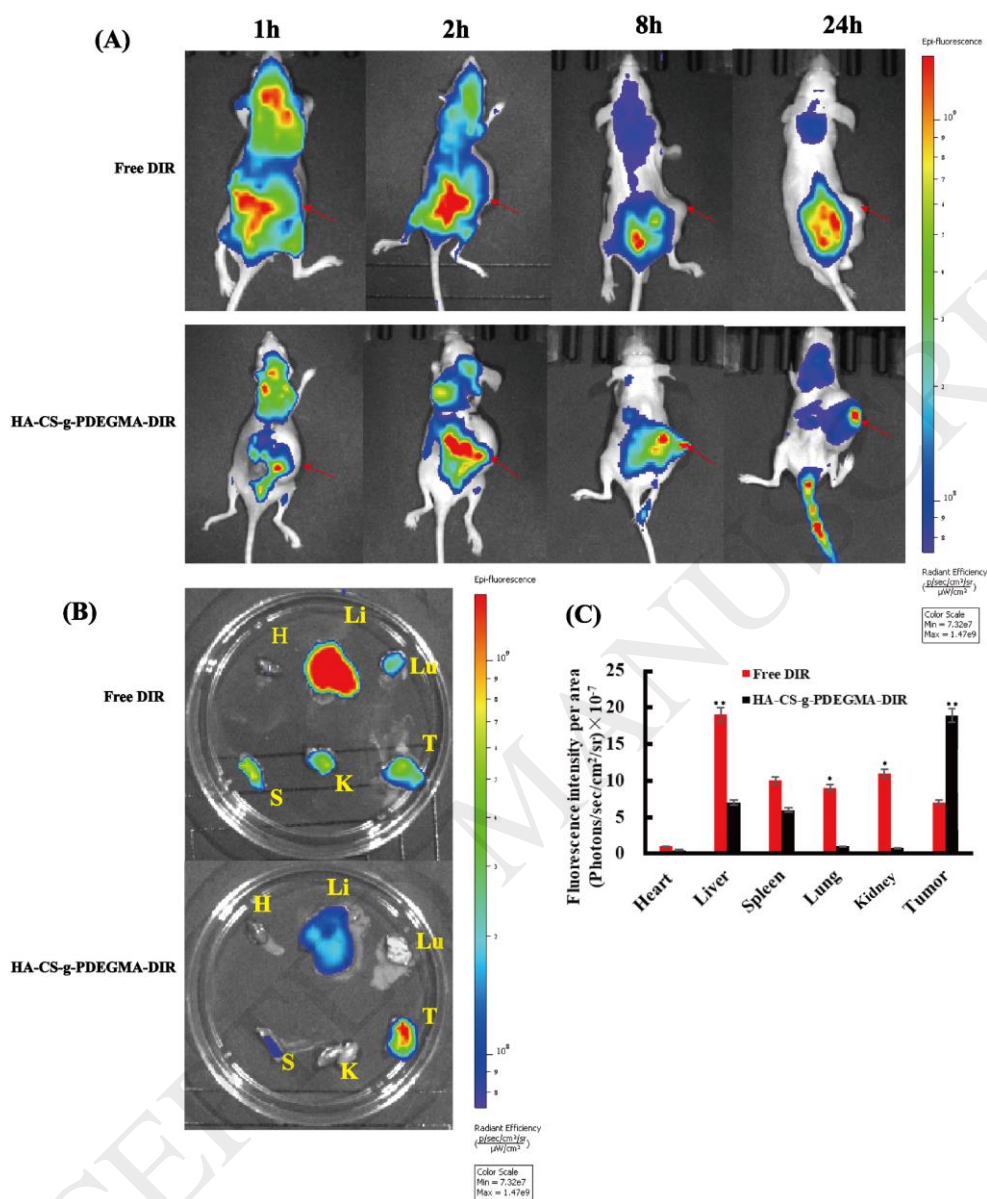


Fig. 6. (A) In vivo fluorescence images of MDA-MB-231 xenograft nude mice after i.v. injection of free DiR and HA-CS-g-PDEGMA-DiR NPs (images taken from different mice). The arrows indicate the tumor foci. (B) Ex vivo images showing the fluorescence intensity in the different organs after 24h, and (C) statistical analysis of hearts (H), livers (Li), spleens (S), lungs (Lu), kidneys (K) and tumors (T) ($n = 8$, results are shown as mean \pm S.D.). * $p < 0.05$, compared with free DiR group; ** $p < 0.01$, compared with free DiR group.

3.7. In vivo therapeutic efficacy and safety

The anticancer properties and toxicity of the NPs were examined using MDA-MB-231 tumor-bearing mice. Images of the tumor blocks isolated on day 30 confirmed that

HA-CS-g-PDEGMA-PTX NPs led to an obvious reduction in tumor size compared to the other groups (Fig. 7A) Tumor volumes were measured during the experiment (Fig. 7B), and mice treated with saline had an average tumor volume of $580 \pm 54 \text{ mm}^3$. Those receiving HA-CS-g-PDEGMA-PTX had mean volumes of $31 \pm 3 \text{ mm}^3$, while the free PTX group had much larger tumors ($199 \pm 17 \text{ mm}^3$). ($p < 0.01$). Body weight data (Fig. 7C) reveal that the body weight of mice in the free PTX group declined with time owing to the systemic toxicity of the drug. In contrast, the saline group show a distinct increase in weight, presumably due to tumor growth. There is only a small increase observable with the NP group. ($p < 0.05$) These results suggest that the HA-CS-g-PDEGMA-PTX NPs have good biocompatibility and could mitigate at least some of the side effects of PTX. These observations are consistent with the findings from in vitro experiments and the in vivo biodistribution studies.

From the Kaplan-Meier survival curves (Fig. 7D), 100% of mice treated with HA-CS-g-PDEGMA-PTX NPs survived over 40 days, and 75% survived for 60 days. However, the mice treated with saline and free PTX all died within 44 days. The NPs prepared in this study offer a notable improvement over similar systems in the literature. For instance, Liu et.al. (Liu et al., 2018) designed a novel self-assembled nanoparticle platform for anticancer drug delivery and noted a 50% mortality rate at 33 days of treatment. The HA-CS-g-PDEGMA-PTX NPs clearly extended the survival time of the mice to a much greater extent.

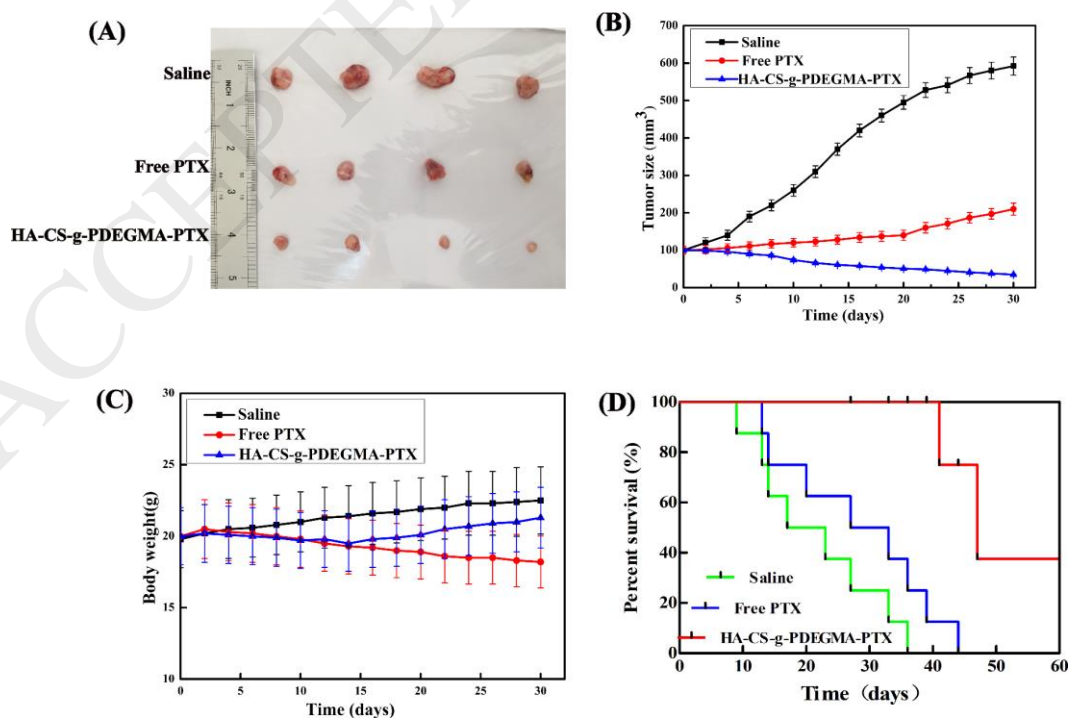


Fig. 7. In vivo tumor model data. (A) Representative photos of tumor tissues resected after 30 days of treatment with saline (control), free PTX, or HA-CS-g-PDEGMA-PTX NPs. (B) Real-time measurements of tumor volume. (C) mean body weights as a function of time. (D) Kaplan-Meier survival curves. * $p < 0.05$, ** $p < 0.01$ compared with HA-CS-g-PDEGMA-PTX NPs group.

3.8. Ex vivo anti-tumor efficacy and systemic toxicity

The major organs and tumors of the mice were excised and visualized by H&E staining after 30 days. As shown in Fig. 8A, mice treated with HA-CS-g-PDEGMA-PTX NPs displayed severe necrosis in the tumor tissue, but minimal damage to the liver (only minor hepatocytic cystic steatosis and some focal inflammation can be seen) and no damage to any other organs. In contrast, the mice treated with free PTX had only slight necrosis in the tumor tissue, but there was severe damage to other organs, including necrocytosis in the spleen, lung and kidney. This is due to the non-selective cytotoxicity of PTX, and the fact that free PTX can accumulate in the major organs because there is no carrier system to target delivery. These results indicate that HA-CS-g-PDEGMA-PTX NPs are more effective than free PTX in treating MDA-MB-231 tumors and have low toxicity to normal tissues.

The TUNEL assay (Fig. 8B) showed there was almost no apoptosis in the tumors of mice treated with saline and only moderate apoptosis in the free PTX group, while HA-CS-g-PDEGMA-PTX NPs induced widespread apoptosis of tumor cells. Quantitative analyses of the TUNEL data are shown in Fig. 8C. After treatment with HA-CS-g-PDEGMA-PTX NPs, the percentage of apoptotic cells in the tumor was $78.4 \pm 6.7\%$, but with the free PTX treatment this value was significantly lower at $41.5 \pm 4.5\%$. These findings, in terms of low systemic toxicity and high degrees of local cell apoptosis in the tumor, accord with other findings in the literature for HA-targeted systems (for instance, the work of Zhong et al. (Zhong et al., 2016) to develop paclitaxel prodrug micelles based on hyaluronic acid-dendritic oligoglycerol).

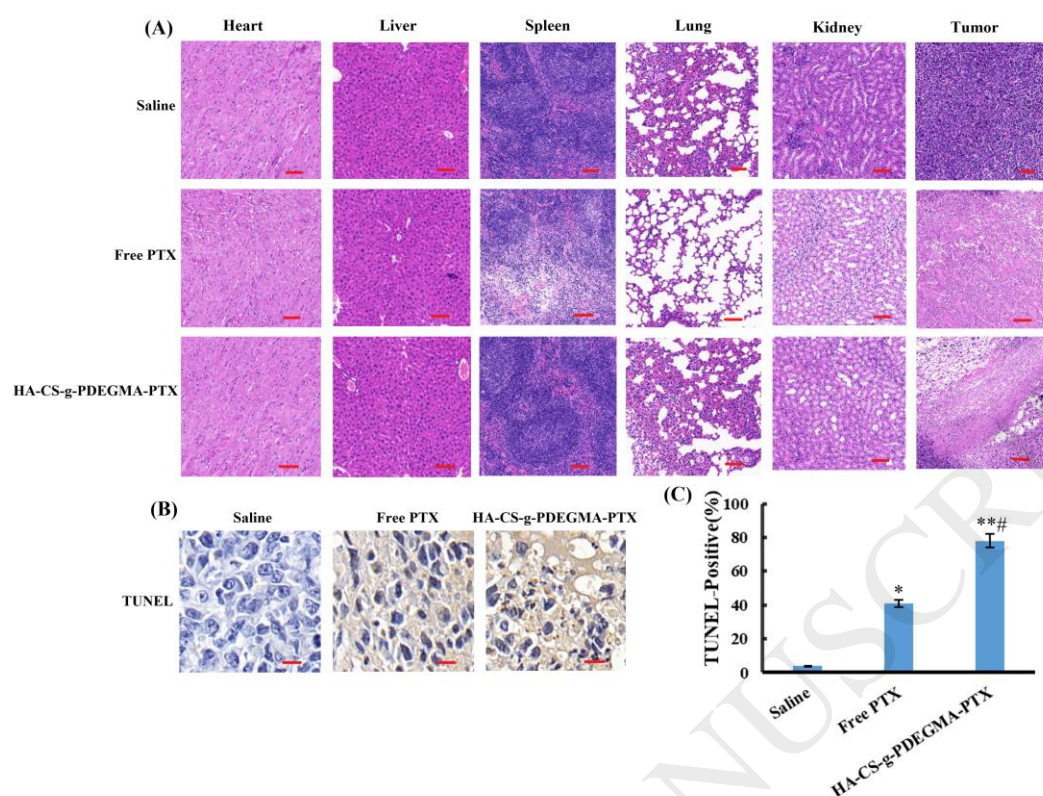


Fig. 8. Histopathology data. (A) sections of heart, liver, spleen, lung, kidney and tumor stained with hematoxylin and eosin. (B) TUNEL staining of tumor sections. Scale bars are 100 μm in the H&E assay and 50 μm in the TUNEL images. (C) Quantitative analysis of the TUNEL positive rates (n = 5, results shown as mean \pm S.D.), * p < 0.05, ** p < 0.01 compared with saline group, #p < 0.05 compared with Free PTX.

4. Conclusions

In this work, novel dual-responsive paclitaxel-loaded nanoparticles (NPs) were successfully synthesized via controlled RAFT polymerization of chitosan and the thermoresponsive monomer di(ethylene glycol) methyl ether methacrylate. The copolymer was able to self-assemble into spherical NPs with a uniform size of around 170 ± 16 nm in water, permitting the NPs to accumulate in tumors via the EPR effect. The NPs showed $13.6 \pm 1.3\%$ drug-loading capacity and $76.2 \pm 8.5\%$ encapsulation efficiency. Hemolysis assays showed that the NPs had good biocompatibility with red blood cells. Confocal microscopy revealed that the NPs can be effectively taken up by cancerous MD-MB-231-cells, and the drug-loaded formulation is highly toxic to these cells. In contrast, there is reduced toxicity to non-cancerous cells. Moreover, the NPs inhibit tumor growth in vivo by inducing apoptosis in the tumor. This is a selective effect, and the NPs exhibit minimal off-target toxicity (in contrast to the administration of paclitaxel itself).

Taken together, our results demonstrate that the NPs prepared in this work comprise a promising therapeutic platform for the treatment of breast cancers.

Disclosure statement

No potential conflict of interests are reported by the authors.

Acknowledgments

This research was financially supported by grant 16410723700 from the Science and Technology Commission of Shanghai Municipality, the Biomedical Textile Materials “111 Project” of the Ministry of Education of China (No. B07024), the UK China Joint Laboratory for Therapeutic Textiles (based at Donghua University) and the National Natural Science Foundation of China (81460647).

References

- Barbuti, A. M., & Chen, Z. S. (2015). Paclitaxel through the ages of anticancer therapy: exploring its role in chemoresistance and radiation therapy. *Cancers*, 7(4), 2360-2371.
- Carelle, N., Piotto, E., Bellanger, A., Germanaud, J., Thuillier, A., & Khayat, D. (2002). Changing patient perceptions of the side effects of cancer chemotherapy. *Cancer*, 95(1), 155-163.
- Chen, C. H., Lin, Y. S., Wu, S. J., & Mi, F. L. (2018). Multifunctional nanoparticles prepared from arginine-modified chitosan and thiolated fucoidan for oral delivery of hydrophobic and hydrophilic drugs. *Carbohydr Polymers*, 193, 163-172.
- de Ligt, K. M., Spronk, P. E. R., van Bommel, A. C. M., Vrancken Peeters, M., Siesling, S., Smorenburg, C. H., & Nabon Breast Cancer Audit, g. (2018). Patients' experiences with decisions on timing of chemotherapy for breast cancer. *Breast*, 37, 99-106.
- Di, Y., Li, T., Zhu, Z., Chen, F., Jia, L., Liu, W., Yang, X. (2017). pH-sensitive and folic acid-targeted MPEG-PHIS/FA-PEG-VE mixed micelles for the delivery of PTX-VE and their antitumor activity. *International Journal Nanomedicine*, 12, 5863-5877.
- Duan, Z., Chen, C., Qin, J., Liu, Q., Wang, Q., Xu, X., & Wang, J. (2017). Cell-penetrating peptide conjugates to enhance the antitumor effect of paclitaxel on drug-resistant lung cancer. *Drug Delivery*, 24(1), 752-764.
- Feng, S.-S., & Chien, S. (2003). Chemotherapeutic engineering: Application and further development of chemical engineering principles for chemotherapy of cancer and other diseases. *Chemical Engineering Science*, 58(18), 4087-4114.
- Hu, B., Wang, S. S., Li, J., Zeng, X. X., & Huang, Q. R. (2011). Assembly of bioactive peptide-chitosan nanocomplexes. *The Journal Physical Chemistry B*, 115(23), 7515-7523.
- Jin, H., Pi, J., & Yang, F. (2016). Folate-chitosan nanoparticles loaded with ursolic acid confer anti-breast cancer activities in vitro and in vivo. *Scientific Reports*, 6, 30782.
- Ke, W., Yin, W., Zha, Z., Mukerabigwi, J. F., Chen, W., Wang, Y., Ge, Z. (2018). A robust strategy for preparation of sequential stimuli-responsive block copolymer prodrugs via thiolactone

- chemistry to overcome multiple anticancer drug delivery barriers. *Biomaterials*, 154, 261-274.
- Kumar, M. N. V. R., Muzzarelli, R. A. A., Muzzarelli, C., Sashiwa, H., & Domb, A. J. (2004). Chitosan chemistry and pharmaceutical perspectives. *Chemical Reviews*, 36(11), 6017-6084.
- Li, F., Pei, D., Huang, Q., Shi, T., & Zhang, G. (2014). Synthesis and properties of novel biomimetic and thermo-responsive dextran-based biohybrids. *Carbohydr Polymers*, 99, 728-735.
- Li, J., Huang, P., Chang, L., Long, X., Dong, A., Liu, J., Deng, L. (2013). Tumor targeting and pH-responsive polyelectrolyte complex nanoparticles based on hyaluronic acid-paclitaxel conjugates and Chitosan for oral delivery of paclitaxel. *Macromolecular Research*, 21(12), 1331-1337.
- Lin, C. W., Lu, K. Y., Wang, S. Y., Sung, H. W., & Mi, F. L. (2016). CD44-specific nanoparticles for redox-triggered reactive oxygen species production and doxorubicin release. *Acta Biomaterialia*, 35, 280-292.
- Liu, Y., Liu, K., Li, X., Xiao, S., Zheng, D., Zhu, P., Wang, L. (2018). A novel self-assembled nanoparticle platform based on pectin-eight-arm polyethylene glycol-drug conjugates for co-delivery of anticancer drugs. *Materials Science Engineering C Materials for Biological Applications*, 86, 28-41.
- Luzon, M., Boyer, C., Peinado, C., Corrales, T., Whittaker, M., Tao, L., & Davis, T. P. (2010). Water-soluble, thermoresponsive, hyperbranched copolymers based on PEG-methacrylates: Synthesis, characterization, and LCST behavior. *Journal of Polymer Science Part A: Polymer Chemistry*, 48(13), 2783-2792.
- Lv, Y., Xu, C., Zhao, X., Lin, C., Yang, X., Xin, X., Yin, L. (2018). Nanoplatform assembled from a CD44-targeted prodrug and smart liposomes for dual targeting of tumor microenvironment and cancer cells. *ACS Nano*, 12(2), 1519-1536.
- Maeda, H. (2001). The enhanced permeability and retention (EPR) effect in tumor vasculature: the key role of tumor-selective macromolecular drug targeting. *Advanced in Enzyme Regulation*, 41(1), 189-207.
- Maeda, H., Wu, J., Sawa, T., Matsumura, Y., & Hori, K. (2000). Tumor vascular permeability and the EPR effect in macromolecular therapeutics: a review. *Journal of Controlled Release*, 65(1), 271-284.
- Mao, H. Q., Roy, K., Troung-Le, V. L., Janes, K. A., Lin, K. Y., Wang, Y., Leong, K. W. (2001). Chitosan-DNA nanoparticles as gene carriers: synthesis, characterization and transfection efficiency. *Journal of Controlled Release Official Journal of the Controlled Release Society*, 70(3), 399-421.
- Marhaba, R., & Zöller, M. (2004). CD44 in cancer Progression: adhesion, migration and growth regulation. *Journal of Molecular Histology*, 35(3), 211-231.
- Martinez-Garcia, M., Vargas-Barron, J., Banuelos-Tellez, F., Gonzalez-Pacheco, H., Fresno, C., Hernandez-Lemus, E., Vallejo, M. (2018). Public insurance program impact on catastrophic health expenditure on acute myocardial infarction. *Public Health*, 158, 47-54.
- Needham, D., & Dewhirst, M. W. (2001). The development and testing of a new temperature-sensitive drug delivery system for the treatment of solid tumors. *Advanced Drug Delivery Reviews*, 53(3), 285-305.
- Nejati, L., Kalantari, F., Bavarsad, N., Saremnejad, F., Moghaddam, P. T., & Akhgari, A. (2018). Investigation of using pectin and chitosan as natural excipients in pellet formulation. *International Journal of Biological Macromolecules*, 120(Pt A), 1208-1215.

- Niu, S., Bremner, D. H., Wu, J., Wu, J., Wang, H., Li, H., Zhu, L. (2018). I-Peptide functionalized dual-responsive nanoparticles for controlled paclitaxel release and enhanced apoptosis in breast cancer cells. *Drug Delivery*, 25(1), 1275-1288.
- Okano, J., & Rustgi, A. K. (2001). Paclitaxel induces prolonged activation of the Ras/MEK/ERK pathway independently of activating the programmed cell death machinery. *Gastroenterology* 120(5), 661-662.
- Pearce, A., Haas, M., Viney, R., Pearson, S. A., Haywood, P., Brown, C., & Ward, R. (2017). Incidence and severity of self-reported chemotherapy side effects in routine care: A prospective cohort study. *PLoS One*, 12(10), e0184360.
- Ramírez-Jiménez, A., Alvarez-Lorenzo, C., Concheiro, A., & Bucio, E. (2014). Temperature-responsiveness and biocompatibility of DEGMA/OEGMA radiation-grafted onto PP and LDPE films. *Radiation Physics and Chemistry*, 99, 53-61.
- Sun, R., Shen, S., Zhang, Y. J., Xu, C. F., Cao, Z. T., Wen, L. P., & Wang, J. (2016). Nanoparticle-facilitated autophagy inhibition promotes the efficacy of chemotherapeutics against breast cancer stem cells. *Biomaterials*, 103, 44-55.
- Tang, J., Hua, D., Cheng, J., Jiang, J., & Zhu, X. (2008). Synthesis and properties of temperature-responsive chitosan by controlled free radical polymerization with chitosan-RAFT agent. *International Journal of Biological Macromolecules*, 43(4), 383-389.
- Tang, S., Meng, Q., Sun, H., Su, J., Yin, Q., Zhang, Z., Li, Y. (2017). Dual pH-sensitive micelles with charge-switch for controlling cellular uptake and drug release to treat metastatic breast cancer. *Biomaterials*, 114, 44-53.
- Torre, L. A., Bray, F., Siegel, R. L., Ferlay, J., Lortet-Tieulent, J., & Jemal, A. (2015). Global cancer statistics, 2012. *Ca A Cancer Journal Clinicians*, 65(2), 87-108.
- Truong, N. P., Whittaker, M. R., Anastasaki, A., Haddleton, D. M., Quinn, J. F., & Davis, T. P. (2016). Facile production of nanoaggregates with tuneable morphologies from thermoresponsive P(DEGMA-co-HPMA). *Polymer Chemistry*, 7(2), 430-440.
- Xing, C., Shi, Z., Tian, J., Sun, J., & Li, Z. (2018). Charge-Determined LCST/UCST Behavior in Ionic Polypeptoids. *Biomacromolecules*, 19(6), 2109-2116.
- Yang, H., Tang, C., & Yin, C. (2018). Estrone-modified pH-sensitive glycol chitosan nanoparticles for drug delivery in breast cancer. *Acta Biomater*, 73, 400-411.
- Yang, Z., Luo, H., Cao, Z., Chen, Y., Gao, J., Li, Y., Liu, J. (2016). Dual-targeting hybrid nanoparticles for the delivery of SN38 to Her2 and CD44 overexpressed human gastric cancer. *Nanoscale*, 8(22), 11543-11558.
- Zhang, P., Zhang, H., He, W., Zhao, D., Song, A., & Luan, Y. (2016). Disulfide-Linked amphiphilic polymer-docetaxel conjugates assembled redox-sensitive micelles for efficient antitumor drug delivery. *Biomacromolecules*, 17(5), 1621-1632.
- Zhong, Y., Goltsche, K., Cheng, L., Xie, F., Meng, F., Deng, C., Haag, R. (2016). Hyaluronic acid-shelled acid-activatable paclitaxel prodrug micelles effectively target and treat CD44-overexpressing human breast tumor xenografts in vivo. *Biomaterials*, 84, 250-261.